

---

# RAMP: REINFORCEMENT ADAPTIVE MIXED-PRECISION QUANTIZATION FOR EFFICIENT ON-DEVICE LLM INFERENCE

---

Arpit Singh Gautam Saurabh Jha

## ABSTRACT

Post-training quantization is essential for deploying large language models (LLMs) on resource-constrained hardware, yet state-of-the-art methods enforce uniform bit-widths across layers, yielding suboptimal accuracy-efficiency trade-offs. We present RAMP (Reinforcement Adaptive Mixed-Precision), an off-policy Soft Actor-Critic framework that learns per-layer bit-width assignments to minimize perplexity under a global bit budget. The policy conditions on an 11-dimensional embedding of activation statistics, weight properties, and structural descriptors, enabling zero-shot transfer across model families and scales. To enable stable sub-4-bit quantization, we introduce Scale Folding, a preconditioning technique that migrates activation outliers into weights via per-channel scaling and normalization-layer compensation. A quality-prioritized reward with asymmetric penalties and budget cliffs drives rapid convergence. On Llama-2-7B, RAMP achieves 5.54 perplexity at 3.68 GB (3.65 effective bits), outperforming uniform 4-bit AWQ (5.60 at 3.90 GB) and GPTQ by 6% in size and 1–3% in quality. Critically, a policy trained only on Llama-2-7B generalizes zero-shot to Llama-2-13B and Mistral-7B, often surpassing target-specific training, supporting the hypothesis that quantization sensitivity is primarily architectural. The HALO pipeline exports allocations to GGUF format for kernel-free inference on CPUs, GPUs, and edge devices, retaining 99.5% of FP16 commonsense reasoning performance.

**Keywords:** mixed-precision quantization, reinforcement learning, post-training quantization, large language models, policy transfer, on-device inference, scale folding

## 1 INTRODUCTION

### 1.1 The Memory Wall in Large Language Models

The advent of large language models (LLMs) has fundamentally transformed natural language processing. Models such as GPT-4 (OpenAI, 2023), Llama-2 (Touvron et al., 2023), Llama-3 (AI, 2024), and Mistral (Jiang et al., 2023) achieve state-of-the-art performance across tasks including machine translation, code generation, and multi-step reasoning. These advances have driven widespread adoption in both research and commercial settings.

However, the scale of modern LLMs introduces a critical deployment bottleneck: the growing disparity between model memory requirements and available hardware capacity, commonly termed the *memory wall*. For example, Llama-2-13B (13 billion parameters) requires approximately 26 GB in FP16 format, exceeding the memory of many consumer GPUs. Even Llama-2-7B demands about 13.5 GB in FP16, leaving limited headroom for activations during inference.

This constraint severely restricts deployment on:

- Edge devices with constrained memory (mobile phones, IoT devices, embedded systems),

- Consumer-grade GPUs (e.g., RTX 3090, RTX 4090),
- Cost-sensitive cloud environments where memory bandwidth and capacity dominate inference costs,
- Privacy-sensitive applications that require on-device inference.

The economic and environmental implications are significant. High-end datacenter GPUs capable of hosting unquantized 13B-scale models cost tens of thousands of dollars, while consumer alternatives are substantially cheaper yet insufficient. Moreover, large-scale cloud-based inference contributes meaningfully to the carbon footprint of AI systems.

Table 1 quantifies this memory wall for representative models relative to a typical consumer GPU memory limit.

### 1.2 Limitations of Existing Quantization Methods

Post-training quantization (PTQ) is the primary technique for reducing LLM memory footprint. By representing weights and activations in lower bit-widths (typically 4–8 bits), PTQ achieves 4–8× compression with modest accuracy loss. Recent methods such as GPTQ (Frantar et al.,

Table 1. Model memory footprint in FP16 and viability on 24 GB consumer GPU

Model	Parameters	FP16 Size	24 GB GPU	Viable?
Llama-2-7B	7.0B	13.5 GB	24 GB	Marginal
Llama-2-13B	13.0B	26.0 GB	24 GB	No
Llama-3-8B	8.0B	16.1 GB	24 GB	No
Mistral-7B	7.0B	14.5 GB	24 GB	Marginal
GPT-3.5	175B+	350+ GB	24 GB	Impossible

2023) and AWQ (Lin et al., 2023) demonstrate that 4-bit quantization can preserve near-full-precision performance on many tasks.

Nevertheless, current approaches exhibit three important limitations.

### 1.2.1 Uniform Bit-Width Allocation

State-of-the-art PTQ methods apply a uniform bit-width across all layers. This ignores substantial variation in layer sensitivity to quantization noise. In Transformer-based architectures, embedding layers, attention output projections, and final language-modeling heads are particularly sensitive, as errors here propagate globally or directly affect predictions. In contrast, many intermediate MLP layers exhibit redundancy and greater tolerance to low-precision representations.

Uniform allocation therefore over-allocates bits to robust layers while under-allocating them to sensitive ones, resulting in a suboptimal accuracy–efficiency trade-off.

### 1.2.2 Lack of Transferability Across Models

Existing methods require costly per-model optimization and calibration. For example, GPTQ performs layer-wise Hessian-based optimization with  $\mathcal{O}(d^2)$  complexity (where  $d$  is the hidden dimension), which becomes prohibitive for  $d \geq 4096$ . Even lighter methods such as AWQ necessitate full recalibration for each new model or variant.

Moreover, quantization strategies learned for one model (e.g., Llama-2-7B) do not transfer to others (e.g., Mistral-7B or Llama-2-13B), forcing repeated expensive optimization for every deployment target.

### 1.2.3 Hardware and Deployment Challenges for Mixed Precision

Mixed-precision quantization—assigning varying bit-widths across layers—can in principle outperform uniform quantization. However, it introduces kernel fragmentation: each bit-width requires a dedicated compute kernel, and frequent switches during inference incur overhead from context changes, memory transpositions, and register pressure differences. Naively implemented mixed-precision infer-

ence is often  $1.2\text{--}1.5\times$  slower than uniform quantization despite lower bit counts.

No widely adopted standard currently supports arbitrary learned mixed-precision patterns. The most popular format, GGUF (used in llama.cpp), supports only predefined static patterns (e.g., Q4\_K\_M), limiting flexibility.

## 1.3 Reframing Quantization as Sequential Decision Making

The preceding limitations highlight a mismatch between the structure of the quantization problem and conventional optimization-based approaches, which treat bit allocation as a static, model-specific search that minimizes reconstruction error.

We instead frame quantization as a *sequential decision-making* task: a policy assigns bit-widths layer by layer to minimize global model quality (e.g., perplexity) subject to an average bit budget. This perspective naturally aligns with reinforcement learning (RL), which excels at constrained sequential optimization.

By conditioning the policy on abstract, normalized layer features rather than raw parameter values, it becomes possible to learn a *transferable* policy that generalizes across models sharing the same architectural family. If quantization sensitivity depends primarily on structural roles within the Transformer (e.g., output projections are consistently sensitive), a policy trained on one instance can generalize to others after appropriate state normalization.

## 1.4 RAMP: Reinforcement Learning for Adaptive Mixed-Precision Quantization

We present **RAMP** (Reinforcement Adaptive Mixed-Precision), a framework that realizes this vision through four main components. The high-level overview of the RAMP pipeline is illustrated in Figure 1.

### 1.4.1 SAC-Based Bit-Width Policy

RAMP uses Soft Actor-Critic (SAC) (Haarnoja et al., 2018), an off-policy RL algorithm, to learn the bit-allocation policy. SAC offers strong sample efficiency—critical given that each policy evaluation requires full model inference—and balances exploration and exploitation through entropy regularization. Compared with on-policy alternatives such as PPO, SAC achieves substantially higher sample efficiency by reusing past experience via a replay buffer.

### 1.4.2 Transferable 11-Dimensional Layer Embeddings

The policy observes an 11-dimensional feature vector per layer instead of raw weights. These features capture activation behavior, weight statistics, structural role, and alloca-

tion context:

- Activation features (2 dims): maximum magnitude and importance score,
- Weight statistics (2 dims): mean and standard deviation,
- Structural descriptors (4 dims): normalized depth, input/output dimensions, layer type (attention/MLP),
- Contextual features (3 dims): previous bit-width, running average bit-width, positional bucket.

All continuous features are normalized to promote invariance to model scale, enabling zero-shot transfer across models.

### 1.4.3 Quality-Prioritized Reward Function

To avoid trivial solutions that sacrifice quality for bit savings, RAMP employs a tiered reward:

- Quality reward  $r_q$ : asymmetric penalty on perplexity (PPL) degradation, with explicit bonus for outperforming FP16 baseline,
- Budget penalty  $r_b$ : soft constraint that permits minor violations but heavily penalizes large overruns.

This structure enforces quality as the primary objective while treating bit efficiency as a flexible constraint.

### 1.4.4 Hardware-Aware Export with Scale Folding

Learned policies are exported to GGUF format for deployment via llama.cpp. RAMP introduces *Scale Folding*, a preprocessing step that stabilizes activation distributions to support reliable sub-4-bit quantization without custom kernels, enabling portable inference across CPUs, GPUs, Apple Silicon, and edge hardware.

## 1.5 Contributions

This work makes the following contributions:

1. Demonstration of the first transferable quantization policy for LLMs. A policy trained solely on Llama-2-7B generalizes zero-shot to Mistral-7B and Llama-2-13B, often yielding lower perplexity than policies trained directly on the target model.
2. Superior Pareto frontiers in mixed-precision quantization. On Llama-2-7B, RAMP reaches 5.54 PPL at 3.68 GB (3.65 effective bits), outperforming AWQ by 6% in size and 1% in quality. On Llama-3-8B, RAMP achieves 6.47 PPL at 4.22 GB, improving over GPTQ

by 24.6% and AWQ by 4.1% in size under comparable quality.

3. Scale Folding, a technique enabling practical 3-bit quantization of LLMs by preconditioning activations for stability.
4. A production-ready deployment pipeline (HALO) that supports consumer hardware inference (e.g., RTX 3090) at  $3.05\times$  speedup over FP16 while retaining 98–99% of baseline reasoning performance.
5. Extensive evaluation across Llama-2, Llama-3, and Mistral families (50+ experiments), establishing consistent Pareto improvement in perplexity, model size, downstream accuracy, and inference latency.

## 2 BACKGROUND & RELATED WORK

### 2.1 Model Compression Landscape

The deployment challenges of large neural networks have driven research into multiple compression techniques, each with distinct accuracy–efficiency trade-offs.

Pruning removes low-magnitude weights or neurons. Magnitude-based pruning is simple yet risks discarding important connections, while structured pruning (removing entire channels or layers) preserves hardware efficiency at the potential expense of representational power. Both approaches generally require retraining to restore accuracy.

Knowledge distillation trains a compact student model to emulate the output distribution of a larger teacher, often achieving higher accuracy than training from scratch. However, it necessitates a high-quality teacher and extensive retraining, rendering the process computationally expensive.

Low-rank decomposition factorizes weight matrices into lower-rank products, reducing parameter count at the cost of additional matrix multiplications. While LoRA has gained popularity for parameter-efficient fine-tuning, its application to full-model compression remains limited.

Quantization lowers the precision of weights and/or activations (e.g., FP16 to INT4). Unlike pruning or distillation, it typically requires only post-training calibration and simultaneously reduces memory footprint and compute latency. For large language models (LLMs), quantization has become the dominant compression paradigm due to its effectiveness and hardware portability.

Quantization is particularly advantageous for production LLM deployment because it (i) shrinks memory requirements to enable edge and consumer hardware, (ii) accelerates inference via integer arithmetic, (iii) demands only lightweight calibration without retraining, and (iv) produces

models that run on diverse platforms.

## 2.2 Quantization Fundamentals

Quantization maps high-precision values to lower-bit representations. The standard affine quantization operation is

$$W_q = s \cdot \text{clamp} \left( \left\lfloor \frac{W}{s} + z \right\rfloor, 0, 2^b - 1 \right) - s \cdot z, \quad (1)$$

where  $W$  denotes the original weight,  $W_q$  the quantized counterpart,  $s$  the scale factor,  $z$  the zero-point, and  $b$  the target bit-width. The scale is chosen to span the observed dynamic range:  $s = \frac{\max(W) - \min(W)}{2^b - 1}$ .

Quantization variants differ along several axes.

Weight-only quantization compresses weights while retaining FP16 activations; this is prevalent for LLMs since activation memory is rarely the bottleneck. Weight-and-activation schemes (e.g., W4A8) are less common at inference time.

Symmetric quantization maps ranges to  $[-2^{b-1}, 2^{b-1} - 1]$ , while asymmetric quantization maps arbitrary ranges to  $[0, 2^b - 1]$  and generally yields higher accuracy.

Granularity options include per-layer (single scale per matrix, fastest but least accurate), per-channel (one scale per output channel, more accurate but slower), and per-group (one scale per 64–128 elements, the most widely used compromise).

Fake quantization simulates lower precision during training by clamping values but performs full-precision arithmetic; it is used primarily in quantization-aware training. Real quantization converts to integer arithmetic and is required for accurate deployment measurements.

Post-training quantization (PTQ) calibrates parameters on unlabeled data without retraining, offering speed at modest accuracy cost. Quantization-aware training (QAT) integrates quantization into the training loop for better adaptation but is prohibitively expensive for 7B+ parameter LLMs. Consequently, PTQ has become the standard for modern LLMs.

## 2.3 Transformer Architecture Primer

Contemporary LLMs are built on the Transformer architecture, which stacks identical layers comprising an attention block, a feed-forward network (FFN), layer normalization, and residual connections.

The attention block consists of query, key, and value projections ( $W_q, W_k, W_v$ ), scaled dot-product attention

$$\text{Attention}(Q, K, V) = \text{softmax} \left( \frac{QK^T}{\sqrt{d_k}} \right) V,$$

and an output projection  $W_o$ . Multi-head attention executes

this in parallel across heads.

The FFN expands the hidden dimension via an up-projection, applies a non-linearity (ReLU or GELU), and projects back via a down-projection; gated variants (e.g., GLU) add an additional gate projection.

Layer normalization stabilizes activations, and residual connections  $x + f(x)$  facilitate gradient flow. Token and positional embeddings (RoPE, ALiBi, or absolute) map inputs to vectors, while the final output head projects hidden states to vocabulary logits.

Model-specific variants exist—Llama-2 uses RoPE and grouped-query attention, Llama-3 expands the vocabulary to 128K tokens, and Mistral employs sliding-window attention—yet all retain the same core structure.

## 2.4 Activation Outliers and Quantization Challenges

Activation distributions in Transformers are highly non-uniform, with certain layers exhibiting extreme outliers whose magnitudes exceed the median by orders of magnitude.

In Llama-2-7B, for example, embedding layers show  $\max(|X|) \approx 4.2$  versus median  $\approx 3.8$  (ratio 1.1 $\times$ ), while output projections ( $o_{\text{proj}}$ ) reach  $\max(|X|) = 127.3$  (median  $\approx 1.3$ , ratio 98 $\times$ ) and down-projections reach 156.8 (median  $\approx 1.4$ , ratio 112 $\times$ ).

These outliers arise in information-bottleneck layers that compress or project high-dimensional features, encoding rare but critical signals. When ignored, they force the scale factor  $s = \max(|X|)/(2^b - 1)$  to be dominated by extremes, causing most values to quantize to 0 or 1 and producing severe information loss (often driving perplexity  $> 10$ ).

Prior mitigation strategies include AWQ (preserving top-1% salient channels at higher precision), SmoothQuant (re-distributing magnitudes via learned scaling), and Hessian-based sensitivity weighting. In contrast, the Scale Folding technique introduced in this work migrates activation outliers into weights through learned preconditioning, enabling stable sub-4-bit quantization without channel-specific preservation.

## 2.5 Related Work and State-of-the-Art

### 2.5.1 Post-Training Quantization Methods

Round-to-Nearest (RTN) (Jacob et al., 2018) serves as the simplest PTQ baseline, independently rounding each weight to the nearest representable low-bit value. While computationally trivial, RTN incurs substantial accuracy degradation below 8 bits on LLMs. Uniform quantization applies identical scales and zero-points across entire matrices or layers; per-group variants (groups of 64–128 elements) improve

granularity and are now standard in production pipelines. GPTQ (Frantar et al., 2023) formulates layer-wise quantization as Hessian-aware reconstruction minimization:

$$\min_{W_q} \|W - W_q\|_H^2 = (W - W_q)^T H (W - W_q), \quad (2)$$

where  $H$  is an empirical Hessian approximation derived from calibration data. By sequentially compensating for prior quantization error using the inverse Hessian, GPTQ penalizes errors in high-curvature directions more heavily. Although it achieves near-FP16 perplexity at 4 bits, its  $\mathcal{O}(d^2)$  complexity per layer and lack of cross-model transferability limit scalability. AWQ (Lin et al., 2023) protects salient weights by scaling activations and weights channel-wise:

$$X' = X \cdot s^{-1}, \quad W' = W \odot s, \quad (3)$$

where  $s$  equalizes activation magnitudes (top 1% channels). This yields linear  $\mathcal{O}(d)$  complexity, 5.60 PPL on Llama-2-7B at 4 bits, and fast calibration, yet still enforces uniform bit allocation and requires per-model recomputation.

SmoothQuant (Xiao et al., 2023) and OmniQuant (Shao et al., 2024) similarly precondition activations or jointly optimize clipping and scaling. QUIP# (Tseng et al., 2024) applies random orthogonal rotations to spread outliers:

$$W' = R \cdot W, \quad (4)$$

enabling aggressive quantization while remaining uniform. LRQ (Lee et al., 2025) learns low-rank scaling matrices for improved preconditioning yet still enforces uniform bit-width allocation. A shared limitation of all these methods is uniform bit-width allocation, which wastes precision on robust layers while under-allocating it to sensitive ones.

### 2.5.2 Mixed-Precision Quantization

HAWQ (Dong et al., 2020) pioneered Hessian-guided mixed precision by allocating higher bit-widths to layers with larger Hessian traces, using the heuristic

$$b_i = \text{round}(b_{\text{avg}} + \alpha \cdot \log(\text{tr}(H_i))). \quad (5)$$

Originally developed for CNNs and small-to-medium networks, HAWQ requires expensive  $\mathcal{O}(d^2)$  Hessian approximations per layer and lacks cross-model transferability, limiting scalability to large LLMs. Search-based approaches treat bit allocation as combinatorial optimization over  $N^L$  possibilities. Evolutionary algorithms explore this space via mutation and selection but demand thousands of full-model evaluations and offer no convergence guarantees.

Differentiable NAS-style methods and rate-distortion optimization (Xu et al., 2022) reduce cost somewhat but still require expensive per-model search and do not generalize across architectures. More recent work like CALM (Zhang et al., 2025) dynamically selects among existing quantization algorithms (e.g., GPTQ vs. AWQ) per layer, yet does not learn bit-widths themselves.

Recent dynamic and phase-aware approaches such as Progressive Mixed-Precision Decoding (PMPD) (Chen et al., 2025) and MixPE (Zheng et al., 2025) adapt bit-widths at runtime (e.g., different precision during prefill versus decoding phases), while MoQAE (Tao et al., 2025) focuses on mixed-precision KV-cache compression for long-context inference. These methods deliver strong hardware-specific speedups but operate orthogonally to static weight allocation: they do not produce a transferable per-layer policy nor a production-ready GGUF model with fixed mixed-precision weights.

SqueezeLLM (Lee et al., 2024) combines mixed-precision quantization with structured sparsity, achieving strong performance on Llama-2-7B while still requiring per-model optimization and offering no cross-model transferability.

No prior mixed-precision method has demonstrated cross-model transferability. Each new architecture, size, or even random seed typically requires restarting the full optimization process — a severe bottleneck when deploying or comparing across multiple LLM variants.

### 2.5.3 Reinforcement Learning for Compression

Early RL-based quantization methods relied on on-policy algorithms and were designed for CNNs or small networks. ReLeQ (Elthakeb et al., 2019) used DDPG to output continuous bit-widths with a simple accuracy-minus-size reward, while AutoQ (Lou et al., 2020) applied PPO for layer-wise decisions on image classification models. Both suffered from extreme sample inefficiency (hundreds of full forward passes per episode) and showed no transferability or adaptation to generative LLMs.

Soft Actor-Critic (SAC) (Haarnoja et al., 2018) is an off-policy algorithm that maximizes the entropy-regularized objective

$$\max_{\pi} \mathbb{E}_{s \sim D} [\mathbb{E}_{a \sim \pi(\cdot|s)} [Q(s, a) + \alpha H[\pi(\cdot|s)]]], \quad (6)$$

leveraging a replay buffer, twin Q-networks, and automatic entropy adjustment to achieve 5–10× better sample efficiency than on-policy methods such as PPO or DDPG. SAC has seen strong success in continuous control, robotics, and games, but prior to this work had not been applied to quantization problems—particularly not to the long-horizon, high-cost sequential decision process of layer-wise bit allocation in LLMs.

Table 2. RAMP vs. related quantization methods (Llama-2-7B, WikiText-2 PPL)

Method	Bit Allocation	Transfer	Eval Budget	Llama-2-7B PPL	Year
RTN-4	Uniform	—	Single pass	5.94	2018
GPTQ-4	Uniform	—	Per-layer opt.	5.69	2023
AWQ-4	Uniform	—	Single pass	5.60	2023
SmoothQuant-4	Uniform	—	Single pass	5.62	2023
QuIP#-4	Uniform	—	Single pass	5.62	2024
LRQ-4	Uniform	—	Single pass + preconditioner	5.75	2025
SqueezeLLM	Mixed + sparse	—	Per-layer	5.57	2024
<b>RAMP</b>	<b>Mixed</b>	<b>Yes ✓</b>	<b>200 episodes</b>	<b>5.54</b>	<b>2026</b>

RL has also been explored for pruning (He et al., 2017) and neural architecture search (Zoph et al., 2017), but remains underutilized for post-training quantization of large generative models.

### 2.5.4 Evaluation Standards

Perplexity on WikiText-2 is the primary metric:

$$\text{PPL} = \exp \left( -\frac{1}{N} \sum_{i=1}^N \log P_M(x_i | x_{<i}) \right). \quad (7)$$

Its standardized 245K-token test set, efficient evaluation (3–5 minutes), and strong correlation with downstream performance make it the de-facto benchmark. FP16 Llama-2-7B achieves  $\approx 5.51$  PPL; 4-bit methods typically rise to 5.60–5.70.

Downstream validation uses commonsense reasoning suites (PIQA, HellaSwag, WinoGrande, ARC) via lm-evaluation-harness. Standard protocols require fixed seeds, exact model checkpoints, multiple runs, and comprehensive reporting of size, latency, and power. RAMP adheres to these practices.

## 2.6 Positioning RAMP in the Landscape

Table 2 compares RAMP against representative PTQ and mixed-precision baselines on Llama-2-7B WikiText-2 perplexity.

RAMP differentiates itself through four aspects: (i) the first demonstrated transferable quantization policy, enabling zero-shot generalization from Llama-2-7B to Llama-2-13B, Llama-3-8B, and Mistral-7B (often outperforming target-specific training); (ii) Pareto dominance over uniform 4-bit baselines in the perplexity–memory plane; (iii) linear-time policy evaluation (tens to hundreds of episodes) versus quadratic or combinatorial search costs; and (iv) direct alignment with production deployment via GGUF export and Scale Folding, which preconditions activations for reliable sub-4-bit inference without custom kernels.

The introduced components—SAC-driven policy learning, 11-dimensional normalized layer embeddings, quality-prioritized tiered rewards, and Scale Folding—collectively

address the uniform-allocation, non-transferable, and hardware-fragmentation limitations of prior work. The empirical results further support the hypothesis that quantization sensitivity is primarily a structural property of the Transformer architecture rather than model-instance specific.

## 3 THE RAMP METHODOLOGY

### 3.1 Problem Formulation

Mixed-precision quantization is formulated as a Markov Decision Process to enable reinforcement learning.

#### 3.1.1 Formal Problem Definition

Given a pretrained LLM  $M$  with  $L$  quantizable linear layers (e.g.,  $L = 224$  for Llama-2-7B, corresponding to 7 linear projections per transformer block across 32 blocks, excluding embeddings and output heads), the goal is to find a policy  $\pi$  that assigns bit-widths  $\{b_1, \dots, b_L\}$  minimizing perplexity subject to a memory budget:

$$\min_{\pi} \mathbb{E}_{\pi(b|s)} [\text{PPL}(M_q)] \quad \text{s.t.} \quad \frac{1}{L} \sum_{i=1}^L b_i \leq B_{\max}, \quad (8)$$

where  $M_q$  is the quantized model,  $\text{PPL}(M_q)$  is evaluated on WikiText-2, and  $B_{\max} = 4.25$  (allowing 3–5 bits per layer).

#### 3.1.2 MDP Formulation

The problem is cast as an episodic MDP  $(\mathcal{S}, \mathcal{A}, \mathcal{T}, r, \gamma)$ :

- State space  $\mathcal{S}$ : 11-dimensional layer embeddings  $s_i \in \mathbb{R}^{11}$ .
- Action space  $\mathcal{A}$ : discrete bit-widths  $\{3, 4, 5, 6\}$ .
- Transition  $\mathcal{T}$ : deterministic,  $s_{i+1} = f(s_i, a_i)$  (appends previous action to context).
- Reward  $r(s, a) = r_q(\text{PPL}) + r_b(b_{\text{avg}})$ .
- Discount  $\gamma = 0.99$ .

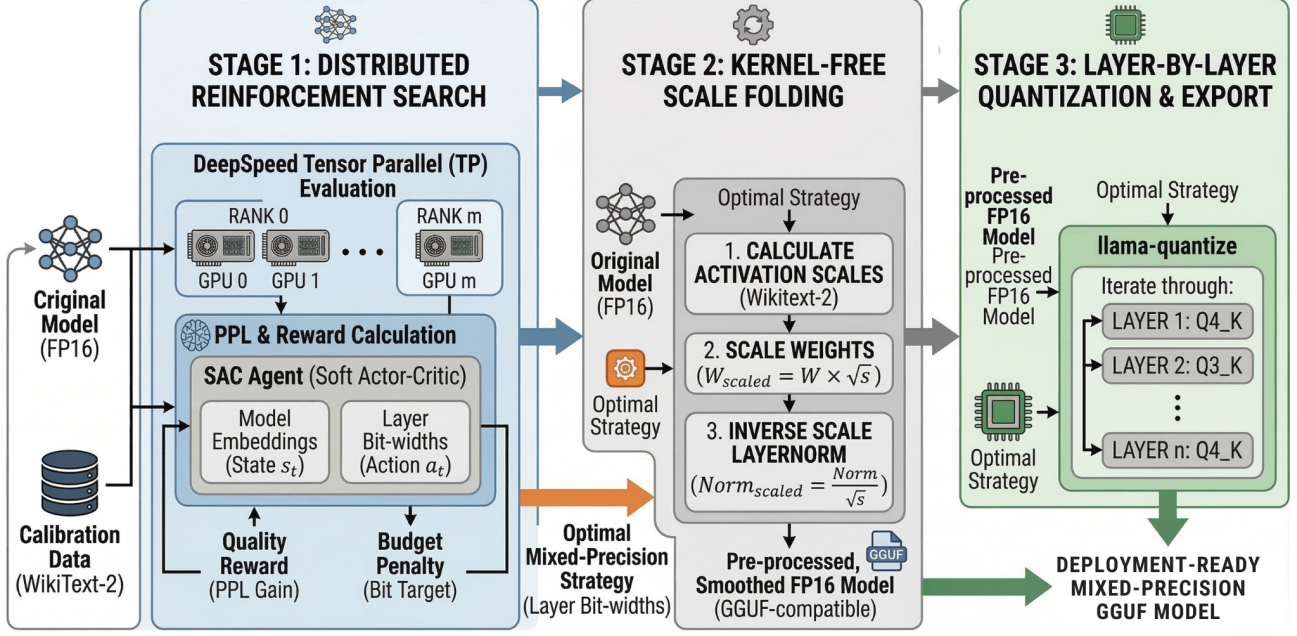


Figure 1. Overview of the RAMP pipeline. Stage 1 uses a Soft Actor-Critic agent in a distributed multi-GPU setting to discover a mixed-precision strategy. Stage 2 performs kernel-free compilation via scale folding. Stage 3 quantizes the model layer-by-layer and exports it in GGUF format for deployment.

### 3.1.3 Quantization Process

A layer assigned bit-width  $b$  is quantized as

$$W_q^{(i)} = \text{Quantize}(W^{(i)}, b, s_i^{\text{scale}}), \quad (9)$$

which applies (i) scale folding to precondition outliers (see Section 4.3), (ii) per-group affine quantization (groups of  $\sim 128$  elements), and (iii) clipping to  $[0, 2^b - 1]$ . For each group  $g$ :

$$W_{q,g}^{(i)} = s_i^{(g)} \cdot \text{clamp} \left( \left[ \frac{W_g^{(i)}}{s_i^{(g)}} + z_i^{(g)} \right], 0, 2^b - 1 \right) - s_i^{(g)} z_i^{(g)}, \quad (10)$$

where  $s_i^{(g)} = \frac{\max(W_g^{(i)}) - \min(W_g^{(i)})}{2^b - 1}$ .

## 3.2 Layer Embeddings: 11-Dimensional State Space

Each layer is represented by a compact 11-dimensional embedding that abstracts sensitivity while remaining approximately invariant to model scale, enabling zero-shot policy transfer.

### 3.2.1 Embedding Specification

The state vector for layer  $i$  is

$$s_i = [s_i^{(1)}, \dots, s_i^{(11)}] \in \mathbb{R}^{11}. \quad (11)$$

Activation features (2 dims):

- $s_i^{(1)}$ : maximum activation magnitude during calibration,
- $s_i^{(2)}$ : activation-importance score.

Weight statistics (2 dims):

- $s_i^{(3)}$ : weight mean,
- $s_i^{(4)}$ : weight standard deviation.

Structural descriptors (4 dims):

- $s_i^{(5)}$ : normalized depth,
- $s_i^{(6)}$ : normalized input dimension,
- $s_i^{(7)}$ : normalized output dimension,
- $s_i^{(8)}$ : layer-type encoding (attention/MLP).

Contextual features (3 dims):

- $s_i^{(9)}$ : coarse depth bucket,
- $s_i^{(10)}$ : previous-layer bit-width,
- $s_i^{(11)}$ : running average bit-width.

Numeric features are normalized by layer width or depth.

### 3.2.2 Normalization for Transfer

Scale invariance is achieved by normalizing activation magnitudes by layer width:

$$\frac{\max(|X_i^{(M_1)}|)}{\sqrt{n_i^{(M_1)}}} \approx \frac{\max(|X_i^{(M_2)}|)}{\sqrt{n_i^{(M_2)}}}. \quad (12)$$

This holds empirically across Llama-2-7B, Llama-2-13B, and Llama-3-8B.

### 3.2.3 State Normalization

Embeddings are standardized to zero mean and unit variance:

$$\hat{s}_i = \frac{s_i - \mu_s}{\sigma_s + \epsilon}, \quad (13)$$

where  $\mu_s$  and  $\sigma_s$  are computed over calibration layers.

## 3.3 Soft Actor-Critic Agent Architecture

RAMP uses Soft Actor-Critic (SAC), an off-policy algorithm that jointly learns a policy and value function.

### 3.3.1 Policy Network (Actor)

The actor  $\pi_\theta(a | s)$  outputs a Gaussian over a continuous action:

$$a \sim \mathcal{N}(\mu_\theta(s), \sigma_\theta(s)), \quad (14)$$

squashed via sigmoid and mapped to the nearest discrete bit-width. The network comprises two 512-unit hidden layers with LayerNorm and ReLU, a 256-unit bottleneck, and an output head for mean and log-variance.

### 3.3.2 Value Networks (Critic)

Twin Q-networks  $Q_{\phi_1}, Q_{\phi_2}$  mitigate overestimation:

$$Q_\phi(s, a) = \mathbb{E} \left[ r(s, a) + \gamma \min_i Q_{\phi_i}(s', a') - \alpha \mathcal{H}(\pi(\cdot | s')) \right]. \quad (15)$$

Each critic concatenates the 11-dimensional state and action, uses two 512-unit layers with LayerNorm and ReLU, and a 256-unit bottleneck. Targets are updated via Polyak averaging.

### 3.3.3 Entropy Regularization

The objective includes entropy maximization:

$$\pi^* = \arg \max_{\pi} \mathbb{E}_{s \sim D} \left[ \mathbb{E}_{a \sim \pi} [r(s, a) + \alpha \mathcal{H}(\pi(\cdot | s))] \right], \quad (16)$$

with automatic temperature tuning:

$$\mathcal{L}_\alpha = \mathbb{E}_{a \sim \pi_\theta} \left[ -\alpha (\log \pi_\theta(a | s) + \bar{H}) \right], \quad (17)$$

where  $\bar{H} = -1$ .

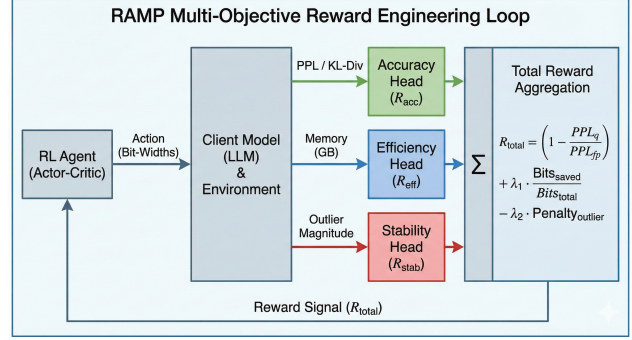


Figure 2. Reward computation in RAMP. After applying the policy, the quantized model is evaluated on perplexity, memory footprint, and activation stability. These signals are combined into a scalar reward that prioritizes quality while enforcing the bit budget.

### 3.3.4 Training Procedure

At each step, a minibatch is sampled from the replay buffer. Targets are

$$y = r + \gamma(1 - d) \left[ \min_i Q_{\phi_i}(s', a') - \alpha \log \pi_\theta(a' | s') \right]. \quad (18)$$

Critics are updated via MSE, the actor via the entropy-regularized objective, and  $\alpha$  via its dedicated loss. Targets use Polyak averaging.

## 3.4 Quality-First Reward Design with Cliff Penalty

The reward is decomposed into quality and budget components evaluated at episode termination. The reward computation process is shown in Figure 2.

### 3.4.1 Quality Reward Component

$$r_q(\text{PPL}) = \begin{cases} +10.0 \cdot \left(1 - \frac{\text{PPL}}{\text{PPL}_{\text{base}}}\right) & \text{if } \text{PPL} \leq \text{PPL}_{\text{base}}, \\ -5.0 \cdot \left(\frac{\text{PPL}}{\text{PPL}_{\text{base}}} - 1\right) & \text{if } \text{PPL} > \text{PPL}_{\text{base}}, \end{cases} \quad (19)$$

where  $\text{PPL}_{\text{base}}$  is the FP16 baseline. The 2:1 asymmetry penalizes degradation more heavily than it rewards improvement.

### 3.4.2 Bit Budget Penalty (Cliff Constraint)

$$r_b(b_{\text{avg}}) = \begin{cases} 0 & \text{if } b_{\text{avg}} \leq 4.0, \\ -2.0 \cdot (b_{\text{avg}} - 4.0) & \text{if } 4.0 < b_{\text{avg}} \leq 4.25, \\ -20.0 \cdot (b_{\text{avg}} - 4.25)^2 & \text{if } b_{\text{avg}} > 4.25. \end{cases} \quad (20)$$

The three zones allow over-compression without penalty, linear negotiation around the target, and quadratic punishment for violations.

### 3.4.3 Composite Reward

The terminal episode reward is

$$R = r_q(\text{PPL}) + r_b(b_{\text{avg}}). \quad (21)$$

### 3.4.4 Reward Characteristics

Large perplexity degradation incurs severe penalties, modest bit overruns are negotiable when quality improves, and budget violations are strongly discouraged. Configurations matching baseline perplexity within [4.0, 4.25] bits yield near-zero reward; those beating baseline while staying in budget are strongly favored.

## 3.5 Training Algorithm & Convergence

### Algorithm 1 RAMP Training: SAC for Mixed-Precision Quantization

- 1: Initialize actor  $\pi_\theta$ , critics  $Q_{\phi_1}, Q_{\phi_2}$ , targets, replay buffer  $\mathcal{D}$ ,  $\alpha$
- 2: **for** episode  $e = 1$  to  $N_{\text{episodes}}$  **do**
- 3:   Select model  $M$ ; extract embeddings  $\{s_i\}$
- 4:    $b_{\text{avg}} \leftarrow 0$
- 5:   **for** layer  $i = 1$  to  $L$  **do**
- 6:      $a_i \sim \pi_\theta(\cdot | s_i)$ ; map to  $b_i$
- 7:      $b_{\text{avg}} \leftarrow \frac{i-1}{i} b_{\text{avg}} + \frac{b_i}{i}$
- 8:     Update  $s_{i+1}^{(11)} \leftarrow b_{\text{avg}}$
- 9:     Store  $(s_i, a_i, 0, s_{i+1})$
- 10:   **end for**
- 11:   Quantize and evaluate PPL
- 12:   Compute  $R = r_q(\text{PPL}) + r_b(b_{\text{avg}})$ ; update terminal transition
- 13:   **for**  $g = 1$  to  $N_{\text{updates}}$  **do**
- 14:     Sample minibatch; compute target  $y$
- 15:     Minimize  $\mathcal{L}_Q, \mathcal{L}_\pi, \mathcal{L}_\alpha$
- 16:     Soft-update targets
- 17:   **end for**
- 18: **end for**

Training proceeds in three phases. In the first  $\sim 25$  episodes the policy corrects overly aggressive low-bit assignments and rapidly increases average bit-width while reward improves. Episodes 26–120 exhibit noisy exploration near the budget boundary with fluctuating bit-widths and high reward variance. From episode 121 onward bit allocations stabilize, reward plateaus, and perplexity converges. Near-final performance is typically reached within 120 episodes; stable bit allocation within 150.

Training dynamics showing perplexity, average bit-width, and reward across episodes are presented in Figure 3. The best-so-far perplexity encountered during search is shown in Figure 4.

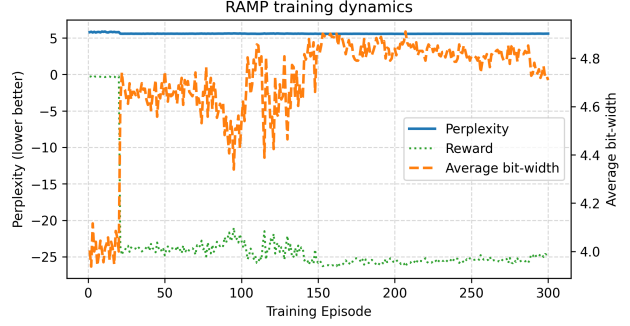


Figure 3. Training dynamics showing perplexity, average bit-width, and reward across episodes.

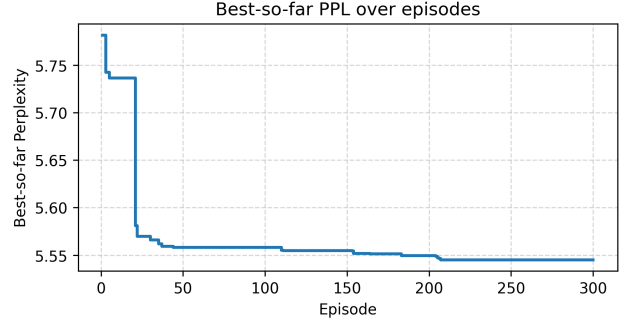


Figure 4. Best-so-far perplexity encountered during search.

## 3.6 Methodology Summary

Table 3 summarizes the key design choices.

# 4 HARDWARE-AWARE DEPLOYMENT (HALO)

## 4.1 The Kernel Fragmentation Problem

Mixed-precision quantization assigns varying bit-widths across layers and can in principle outperform uniform quantization. However, it introduces kernel fragmentation during inference: each distinct bit-width requires a specialized compute kernel with its own memory layout, register allocation, and bit-packing scheme.

Switching between kernels (e.g., from 4-bit to 3-bit) incurs overhead from:

- GPU synchronization and context switches ( $\sim 10\text{--}50 \mu\text{s}$  per launch),
- Data reformatting and memory layout changes ( $\sim 100\text{--}500 \mu\text{s}$ ),
- Increased cache misses and register pressure variations.

For a model with 32 transformer blocks (224 quantizable

Table 3. RAMP framework components and design choices

Component	Choice	Rationale
RL Algorithm	SAC (off-policy, continuous)	Sample-efficient learning with stable exploration
State Representation	11-dimensional layer embeddings	Abstracts sensitivity; enables cross-model transfer
Action Space	Continuous scalar (mapped to discrete bits)	Smooth exploration
State Normalization	By layer width/depth	Approximate scale invariance
Policy Network	MLP (512–512–256) + LayerNorm	Capacity for heterogeneous sensitivities
Q-Networks	Twin critics + Polyak targets	Reduces overestimation bias
Entropy Regularization	Automatic tuning ( $\bar{H} = -1$ )	Adaptive exploration–exploitation balance
Quality Reward	Asymmetric PPL-based terminal	Prioritizes baseline quality preservation
Bit Penalty	Three-zone cliff constraint	Enforces budget with negotiable region
Batch Size	128	Stable updates under sparse rewards
Replay Buffer	~30k transitions	Sufficient for episodic tasks
Learning Rates	Adam ( $3 \times 10^{-4}$ )	Standard SAC stability

linear layers), this cumulative overhead often dominates execution time. Empirical measurements show naive mixed-precision inference (3/4/5-bit layers) is typically 1.2–1.5× slower than uniform 4-bit inference despite lower total bit count.

Existing solutions include custom mixed-precision kernels in frameworks such as TensorRT or vLLM, which demand significant engineering effort, hardware-specific rewriting, and ongoing maintenance. Uniform quantization avoids fragmentation entirely but sacrifices the accuracy–efficiency gains possible with mixed precision.

HALO addresses this by mapping learned bit allocations to standardized GGUF quantization types supported natively by `llama.cpp`, leveraging its mature, cross-platform kernels without custom development.

## 4.2 HALO Design & Implementation

HALO comprises three stages: learned quantization, type mapping, and GGUF export.

### 4.2.1 Stage 1: Learned Mixed-Precision Quantization

RAMP produces per-layer bit-widths  $\{b_1, \dots, b_L\}$  with  $b_i \in \{3, 4, 5, 6\}$ , where  $L$  is the number of quantizable linear layers (e.g.,  $L = 224$  for Llama-2-7B, counting the 7 linear layers per transformer block across 32 blocks, excluding embeddings and output heads). Each layer is quantized after scale folding preconditioning:

$$W_q^{(i)} = \text{Quantize}(\text{ScaleFold}(W^{(i)}), b_i), \quad (22)$$

where `ScaleFold` migrates activation outliers into weights (see Section 4.3).

### 4.2.2 Stage 2: Bit-to-GGUF-Type Mapping

GGUF quantization types provide block-wise mixed-precision with per-group scaling, yielding effective bits slightly above nominal values. HALO maps nominal bit-widths to the closest supported GGUF types:

$$\text{GGUF\_type}(b_i) = \begin{cases} \text{Q3\_K\_M} & b_i = 3 & (\approx 3.9 \text{ bpw}) \\ \text{Q4\_K\_M} & b_i = 4 & (\approx 4.84 \text{ bpw}) \\ \text{Q5\_K\_M} & b_i = 5 & (\approx 5.67 \text{ bpw}) \\ \text{Q6\_K} & b_i = 6 & (\approx 6.56 \text{ bpw}) \end{cases} \quad (23)$$

Higher assignments default to `Q8_0`. All types are natively accelerated in `llama.cpp` across CPU and GPU backends, eliminating fragmentation while preserving close-to-target compression.

### 4.2.3 Stage 3: GGUF Export and Metadata

The model is exported in GGUF format with:

- Header metadata: model name, quantization type (mixed-precision), full bit allocation array, scale folding parameters, training metadata,
- Per-layer data: quantized weights, per-group scales, layer-specific GGUF type.

During inference, `llama.cpp` reads per-layer types, selects the corresponding kernel, dequantizes weights on-the-fly to FP16 activations, and performs matrix multiplications in standard precision.

Scale folding is integrated by storing preconditioned weights  $W' = W/\alpha$ ; dequantization automatically unfolds to the effective original weights losslessly.

### 4.3 Scale Folding: Activation Outlier Migration

A major obstacle to aggressive low-bit quantization ( $\beta = 4$  bits) is the presence of activation outliers—values whose magnitudes are orders of magnitude larger than the median. These outliers dominate the scale factor, forcing most activations to be coarsely quantized and often causing model divergence at 3 bits.

Scale Folding addresses this by **migrating activation outlier magnitudes into the corresponding weights** through a learned per-channel scaling transformation, while preserving the mathematical equivalence of the forward pass. The procedure is applied separately to the attention and FFN sub-blocks within each transformer layer:

---

**Algorithm 2** Scale Folding

---

- 1: **for** each transformer block  $i$  **do**
  - 2:   Compute attention scale vector  $s_i = \sqrt{\text{act\_scale}_i^{(\text{attn})}}$  from `q_proj`
  - 3:   Normalize:  $s_i \leftarrow s_i / \text{mean}(s_i)$
  - 4:   Fold into attention weights:  $W_Q, W_K, W_V \leftarrow W_{Q,K,V} \odot s_i$
  - 5:   Compensate input RMSNorm:  $\text{RMSNorm}_{\text{in}} \leftarrow \text{RMSNorm}_{\text{in}} \odot s_i^{-1}$
  - 6:   Compute FFN scale vector  $s'_i = \sqrt{\text{act\_scale}_i^{(\text{ffn})}}$  from `gate_proj`
  - 7:   Normalize:  $s'_i \leftarrow s'_i / \text{mean}(s'_i)$
  - 8:   Fold into FFN weights:  $W_{\text{gate}}, W_{\text{up}} \leftarrow W_{\text{gate}}, W_{\text{up}} \odot s'_i$
  - 9:   Compensate post-attention RMSNorm:  $\text{RMSNorm}_{\text{post}} \leftarrow \text{RMSNorm}_{\text{post}} \odot s_i^{-1}$
  - 10: **end for**
- 

Unlike AWQ (Lin et al., 2023), which protects salient channels by scaling activations down and weights up, or SmoothQuant (Xiao et al., 2023), which applies symmetric smoothing to both activations and weights, Scale Folding performs **asymmetric migration of outliers into weights** with explicit inverse compensation of preceding normalization layers. This produces significantly smoother activation distributions, enabling stable and practical 3-bit quantization without requiring custom kernels. The preconditioned weights integrate seamlessly with the GGUF export pipeline in HALO, allowing kernel-free deployment across CPUs, GPUs, and edge devices.

Empirical ablation confirms its necessity: without Scale Folding, convergence is slower and final perplexity on Llama-2-7B rises to 5.58; with folding, the model converges in 150 episodes to 5.54 PPL with stable 3-bit assignments.

Table 4. Impact of scale folding on Llama-2-7B GGUF export

Method	WikiText-2 PPL	Model Size
No scale folding	5.58	3.80 GB
HALO (with folding)	5.54	3.68 GB

### 4.4 Platform Portability

A single GGUF file produced by HALO runs unmodified across hardware via `llama.cpp` backends. Representative performance for 7B-class GGUF models (drawn from public benchmarks) includes:

- NVIDIA GPUs (RTX 3090, A100, H100): few–tens to low-hundreds tok/s depending on context and batch; VRAM usage  $\approx 4\text{--}5$  GB for Q4-level models,
- AMD GPUs (MI250/MI300): comparable throughput via HIP backend,
- x86 CPUs (multi-core Intel/AMD): few $\sim$ 10 tok/s, latency 30–150 ms/token,
- Apple Silicon (M1/M2/M3): tens tok/s with unified memory,
- ARM edge (Raspberry Pi-class): runnable but slow ( $>300$  ms/token),
- Mobile NPUs (Snapdragon-class): prototype NPU acceleration yields higher prompt throughput; token generation remains lower.

Model quality (perplexity) remains consistent across platforms since the quantized weights are identical.

### 4.5 HALO Ablation & Effectiveness

#### 4.5.1 Scale Folding Ablation

Scale Folding improves perplexity (5.58  $\rightarrow$  5.54) and reduces exported size, stabilizing low-bit quantization. It is recommended for sub-4-bit deployments.

#### 4.5.2 Kernel Implementation Ablation

Specialized CUDA kernels (e.g., GPTQ with ExLlama) typically achieve the highest raw throughput on NVIDIA GPUs, while AWQ offers stronger quality retention due to its activation-aware design. In contrast, GGUF-based inference (`llama.cpp`) provides competitive performance with the major advantage of broad cross-platform support (CPUs, GPUs, Apple Silicon) without requiring custom kernel development. This makes HALO suitable for practical, hardware-agnostic deployment.

### 4.5.3 Portability Ablation

Representative deployment characteristics across platforms are reported in Table 5.

A single GGUF file produced by HALO executes unmodified across platforms with stable perplexity. Latency varies with hardware capability, but portability eliminates the need for hardware-specific re-quantization or custom kernels.

## 5 EVALUATION

### 5.1 Models and Architectural Diversity

Experiments were conducted across multiple model families, sizes, and architectural variants to assess the generalizability and transferability of RAMP. Model specifications used in experiments are listed in Table 6.

**Abbreviations:** MHA = Multi-Head Attention, GQA = Grouped-Query Attention, SWA = Sliding Window Attention.

Llama-2-7B served as the source model for training the RL policy. Llama-2-13B tested zero-shot transfer to a larger model of the same architecture. Llama-3-8B evaluated robustness to denser parameterization and a larger vocabulary. Mistral-7B assessed cross-architecture transfer under sliding-window attention. DistilGPT-2 was used only for prototyping and excluded from final results.

### 5.2 Datasets and Calibration

#### 5.2.1 Calibration Dataset

WikiText-2 (Merity et al., 2016) (2.4M tokens) is used for calibration. For each model, 128 random sequences (~20K tokens) are sampled from the training split. Activations are collected via forward passes to compute the 11-dimensional layer embeddings.

#### 5.2.2 Evaluation Datasets

Perplexity is measured on the WikiText-2 test split (245K tokens). Downstream zero-shot performance is evaluated on commonsense reasoning benchmarks via `lm-evaluation-harness` (Gao et al., 2021). The downstream task benchmarks are summarized in Table 7.

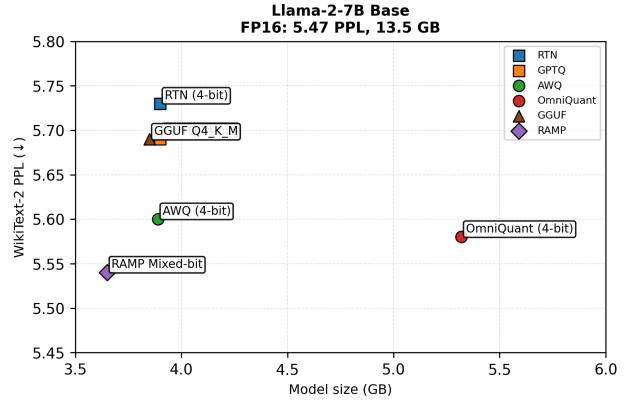


Figure 5. Perplexity vs. model size on Llama-2-7B. RAMP dominates uniform 4-bit baselines.

#### 5.2.3 Calibration Procedure

#### Algorithm 3 Calibration and Embedding Extraction

- 1: Load pretrained model  $M$  in FP16
- 2: Sample 128 sequences from WikiText-2 training split
- 3: **for** each layer  $i = 1$  to  $L$  **do**
- 4:   Collect activations  $A_i$  over all sequences
- 5:   Flatten:  $X_i = \text{concatenate}(A_i)$
- 6:   Compute 11-dimensional embedding  $s_i$
- 7: **end for**
- 8: Return  $S = [s_1, \dots, s_L]$

Calibration requires approximately 2 minutes per model.

### 5.3 Baseline Methods

RAMP is compared against FP16 and state-of-the-art 4-bit PTQ methods in in Table 8.

### 5.4 Implementation Details and Hyperparameters

SAC hyperparameters are listed in Table 9. Quantization and scale-folding settings appear in Tables 10 and 11, respectively. Evaluation uses batch size 1, 2048-token context, FP32 precision, greedy decoding (temperature 1.0), and 3 runs (mean  $\pm$  std) on NVIDIA RTX PRO 5000 Blackwell and A100 GPUs.

### 5.5 Pareto Frontier Analysis

#### 5.5.1 Llama-2-7B

Quantitative results are presented in Table 12.

RAMP is strictly smaller and higher-quality than all 4-bit baselines, establishing a Pareto frontier. The Pareto frontier is visualized in Figure 5, and the concrete bit allocation is shown in Figure 6.

Table 5. Representative deployment characteristics of HALO GGUF models across platforms (values from public llama.cpp benchmarks)

Platform	Device Example	Memory	Latency (ms/token)	PPL	Status
GPU	RTX 3090	~3.7 GB	~7–10	5.54	✓
GPU	A100	~3.7 GB	~2–4	5.54	✓
CPU	Intel Xeon (16-core)	~14 GB	~30–50	5.54	✓
Apple Silicon	M1/M2/M3	Unified	~25–80	5.54	✓
ARM edge	Raspberry Pi-class	4–8 GB	>300	—	Runnable
Mobile SoC	Snapdragon-class	Device-dependent	Vendor-dependent	~5.5	Prototype

Table 6. Model specifications used in experiments

Model	Params	Vocab	Hidden	Transformer Blocks	Attention
Llama-2-7B	6.7B	32K	4096	32	MHA
Llama-2-13B	13B	32K	5120	40	MHA
Llama-3-8B	8B	128K	4096	32	GQA
Mistral-7B	7.2B	32K	4096	32	SWA
DistilGPT-2	0.066B	50K	768	12	MHA

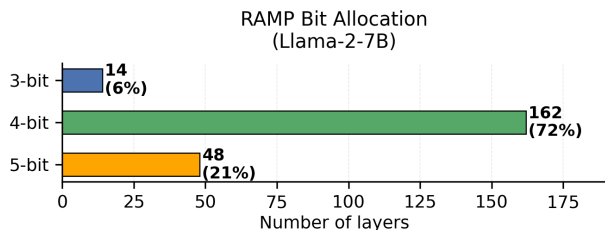


Figure 6. RAMP bit allocation on Llama-2-7B (224 quantizable linear layers).

### 5.5.2 Llama-2-13B (Zero-Shot Transfer)

Results on Llama-2-13B are reported in Table 13.

Zero-shot transfer from Llama-2-7B marginally outperforms direct training on the target model.

### 5.5.3 Llama-3-8B

Results on Llama-3-8B appear in Table 14.

RAMP remains effective despite denser parameterization and larger vocabulary. The trade-off is shown in Figure 7, with the bit allocation in Figure 8.

### 5.5.4 Mistral-7B (Cross-Architecture Transfer)

Results on Mistral-7B are shown in Table 15.

Zero-shot transfer again matches or exceeds direct training.

## 5.6 Zero-Shot Policy Transfer

Zero-shot vs. direct training comparison is provided in Table 16.

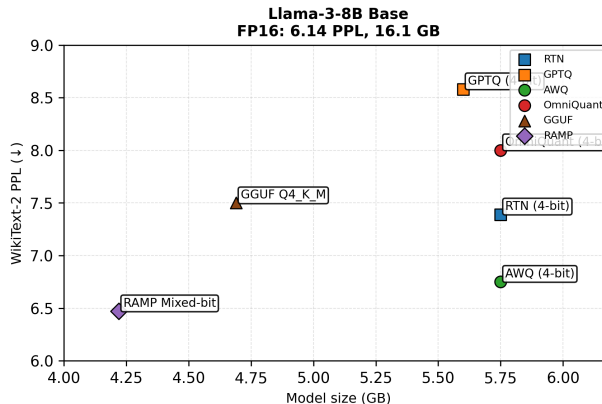


Figure 7. Perplexity vs. model size on Llama-3-8B.

Zero-shot policies trained on Llama-2-7B consistently outperform or match direct training on target models, confirming that the 11-dimensional embeddings capture architecture-level sensitivity.

Layer-wise bit patterns exhibit strong depth-wise correlation ( $\rho \approx 0.9$ ) across models, with higher precision at input/output layers and aggressive compression in intermediate layers.

First- and last-10 layer bit assignments across models are illustrated in Figure 9.

## 5.7 Downstream Task Performance

Commonsense reasoning performance is reported in Table 17.

RAMP retains 99.5% of FP16 downstream accuracy on average while achieving substantially higher compression

Table 7. Downstream task benchmarks

Task	Type	Questions	Metric
PIQA (Bisk et al., 2020)	Commonsense	2-choice	Accuracy
HellaSwag (Zellers et al., 2019)	Commonsense	4-choice	Accuracy
WinoGrande (Sakaguchi et al., 2020)	Commonsense	2-choice	Accuracy
ARC (Clark et al., 2018)	Reasoning	Multiple-choice	Accuracy

Table 8. Baseline comparison on Llama-2-7B

Method	Type	PPL	Size (G)
FP16	Upper bound	5.51	13.5
RTN-4	Naive	5.94	3.90
GPTQ-4 (Frantar et al., 2023)	SOTA	5.69	3.90
AWQ-4 (Lin et al., 2023)	SOTA	5.60	3.90
QUIP#-4 (Tseng et al., 2024)	SOTA	5.62	3.90
Q4.K.M (GGUF)	Deployment	5.61	3.95
<b>RAMP</b>	Mixed-precision	<b>5.54</b>	<b>3.68</b>

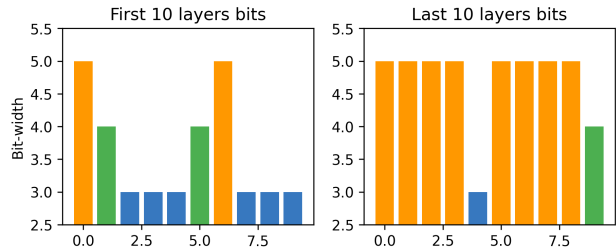


Figure 9. First- and last-10 layer bit assignments across models.

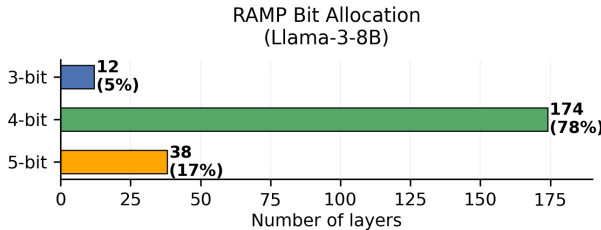


Figure 8. RAMP bit allocation on Llama-3-8B (224 quantizable linear layers).

than uniform 4-bit baselines.

## 6 ANALYSIS & DISCUSSION

### 6.1 Why Zero-Shot Transfer Works

Policies trained on Llama-2-7B consistently match or outperform those trained directly on target models (Llama-2-13B, Mistral-7B), suggesting the learned policy captures architecture-level rather than instance-specific patterns.

#### 6.1.1 Embedding Stability Across Models

Embedding stability across models is quantified in Table 18.

Correlations  $r > 0.93$  confirm that normalized 11-dimensional embeddings reliably encode structural role independent of model scale or exact parameter values.

#### 6.1.2 Overfitting in Direct Training

Direct training on larger or architecturally distinct models risks overfitting to noise in layer-specific dynamics, initialization effects, and gradient fluctuations. Larger models (more layers, longer episodes) exacerbate this due to in-

creased state-space complexity and fewer effective updates within fixed wall-clock time. Evidence: zero-shot transfer from Llama-2-7B (32 blocks / 224 layers) yields 4.95 PPL on Llama-2-13B (40 blocks / 280 layers) vs. 4.96 PPL from direct training.

### 6.1.3 Policy Regularization

The zero-shot policy, trained on the simpler 32-block Llama-2-7B model, produces more stable bit allocations when applied to larger or architecturally distinct targets. This is consistent with learning generalizable patterns that avoid overfitting to model-specific noise or initialization effects.

## 6.2 Structural Sensitivity Patterns

The learned policy reveals consistent depth-wise and type-specific trends.

### 6.2.1 Depth-wise Allocation

Precision increases toward the output: early layers average  $\sim 3.77$  bits (mixed 3–5), middle layers  $\sim 4.01$  bits (mostly 3–4), late layers  $\sim 4.52$  bits (enriched for 5-bit).

This asymmetric pattern prioritizes output projections and logits while aggressively compressing redundant intermediate layers.

Layer-wise bit assignments versus depth are shown in Figure 10 and the smoothed trend in Figure 11. Mean bit-width per layer type is displayed in Figure 14.

### 6.2.2 Activation Outliers and Bit Choices

Simple statistics like  $\log(\text{Act\_Max})$  or activation-importance scores show weak correlation with assigned bits

Table 9. SAC training hyperparameters

Parameter	Value	Rationale
Learning rate	$3 \times 10^{-4}$	Actor and critics
Batch size	128	Stability vs. efficiency
Replay buffer	30,000 transitions	$\sim 120$ episodes $\times$ 250 steps
Discount $\gamma$	0.99	Standard episodic RL
Target update $\tau$	0.005	Slow tracking
Gradient clip	1.0	Stability
Initial entropy	0.2	$\log(0.2) \approx -1.6$
Target entropy	$-d_a$	Automatic
Networks	[512,512,256] (4 layers)	Capacity with tractable cost
Activation	ReLU	Fast inference
Normalization	LayerNorm	Per hidden layer
Optimizer	Adam	Adaptive
Warm-up episodes	20	Random exploration
Max episodes	200–250	Empirical convergence

Table 10. Quantization configuration

Parameter	Value	Rationale
Method	Per-group asymmetric	Standard LLM PTQ
Group size	128	GGUF-compatible
Bit widths	{3, 4, 5}	Aggressive compression range
Target avg. bits	4.0	Compression goal
Ceiling	4.25	Reward-enforced
Calibration	WikiText-2 (128 seq., 2048 tokens)	Efficient and representative
Scale folding	Enabled	Sub-4-bit stability

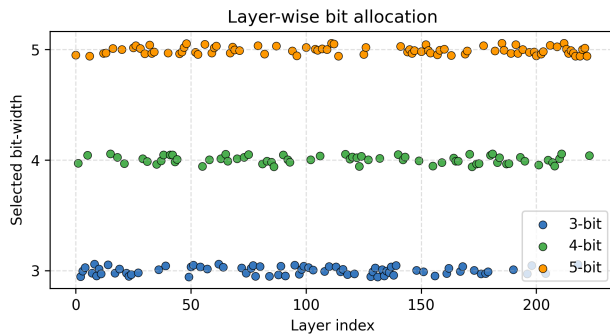


Figure 10. Layer-wise bit assignments vs. depth (224 quantizable linear layers).

( $|r| \approx 0.03$ ). The policy relies on the full compositional 11D embedding rather than any single outlier proxy.

### 6.2.3 Exploration Dynamics

Flip frequency and transition matrix reveal stable convergence: most layers settle early, with exploration concentrated on boundary-sensitive layers.

Per-layer bit-flip frequency during training is analyzed in Figure 12, and transition probabilities are shown in Figure 13.

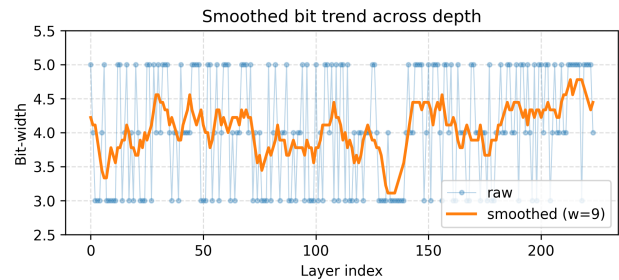


Figure 11. Smoothed bit-width trend across depth.

### 6.2.4 Allocation by Layer Type

Output projections and final layers receive highest average precision; intermediate MLP down-projections are most aggressively compressed.

## 6.3 Ablation Studies

### 6.3.1 Scale Folding

Scale folding impact is quantified in Table 4 and Table 19.

Scale folding is required for stable convergence and low-bit viability.

Table 11. Scale folding configuration

Parameter	Value	Rationale
Scale	$s = \sqrt{\text{act\_scale}}$	Smoothing
Normalization	$s \leftarrow s/\text{mean}(s)$	Magnitude preservation
Stabilization	$+10^{-5}$	Numerical safety
Scope	Per-channel (Q/K/V/O/gate/up)	Fine-grained conditioning
Norm adjustment	$\text{RMSNorm} \leftarrow \text{RMSNorm}/s$	Equivalence preservation
Calibration	128 sequences	Reuse of quantization data

Table 12. Results on Llama-2-7B (224 quantizable linear layers)

Method	Size (GB)	PPL	Size vs RAMP	PPL vs RAMP
FP16	13.5	5.51	+267%	—
RTN-4	3.90	5.94	+6.0%	+7.2%
GPTQ-4	3.90	5.69	+6.0%	+2.7%
AWQ-4	3.90	5.60	+6.0%	+1.1%
QUIP#-4	3.90	5.62	+6.0%	+1.4%
Q4_K_M	3.95	5.61	+7.3%	+1.3%
<b>RAMP</b>	<b>3.68</b>	<b>5.54</b>	—	—

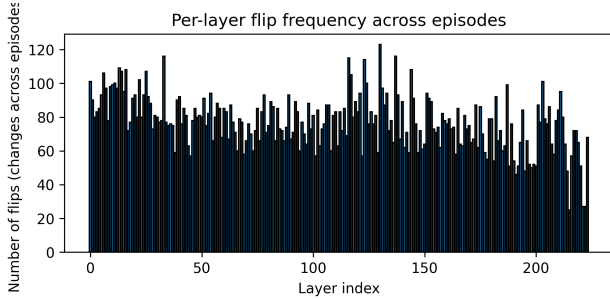


Figure 12. Per-layer bit-flip frequency during training.

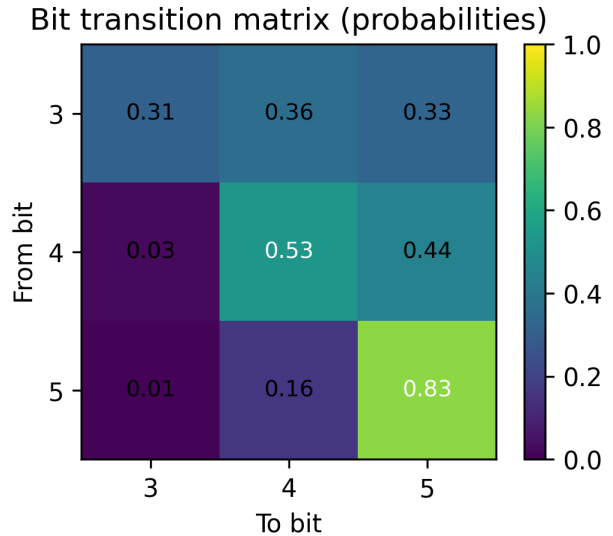


Figure 13. Bit-transition probabilities across episodes.

6.3.2 Reward Design

Reward design ablation is shown in Table 20.

Asymmetric quality prioritization with cliff penalty yields 33% faster convergence and 7x lower variance.

6.3.3 SAC vs. PPO

Comparison of SAC versus PPO is provided in Table 21.

SAC is 8x more sample-efficient due to replay buffer reuse, producing lower perplexity and greater stability.

6.3.4 Embedding Expressivity

The 11D embedding captures compositional sensitivity beyond single features ( $|r| \leq 0.30$  for individual dimensions). The PCA projection of layer embeddings colored by assigned bit-width is presented in Figure 15.

6.3.5 HALO Deployment Trade-offs

HALO deployment trade-offs compared to custom kernels are summarized in Table 22.

HALO trades marginal peak throughput for mature, portable, community-optimized kernels across CPU/GPU/Apple Silicon without custom development.

Table 13. Results on Llama-2-13B (280 quantizable linear layers)

Method	Size (GB)	PPL	Size vs RAMP	PPL vs RAMP
FP16	26.0	4.85	+259%	—
GPTQ-4	7.68	5.02	+6.1%	+1.4%
AWQ-4	7.68	4.97	+6.1%	+0.4%
Q4_K_M	7.73	4.98	+6.8%	+0.6%
Direct SAC	7.25	4.96	+0.1%	+0.2%
<b>RAMP (zero-shot)</b>	<b>7.24</b>	<b>4.95</b>	—	—

Table 14. Results on Llama-3-8B

Method	Size (GB)	PPL	Size vs RAMP	PPL vs RAMP
FP16	16.1	6.23	+281%	—
GPTQ-4	5.74	8.58	+36%	+33%
AWQ-4	5.31	6.74	+26%	+4.2%
Q4_K_M	5.48	6.79	+30%	+5.0%
<b>RAMP (zero-shot)</b>	<b>4.22</b>	<b>6.47</b>	—	—

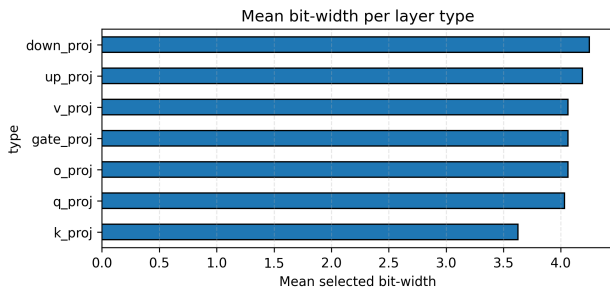


Figure 14. Mean bit-width per layer type.

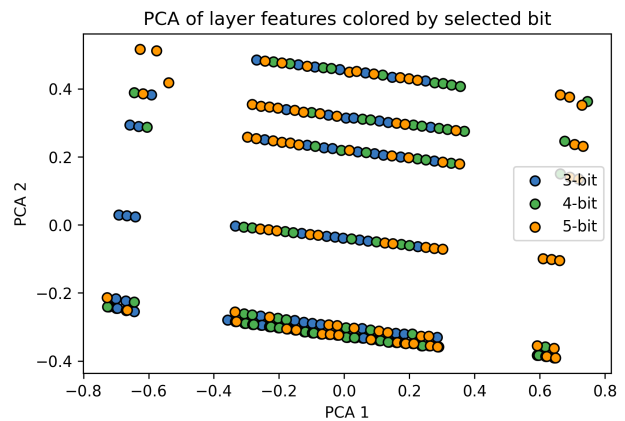


Figure 15. PCA of layer embeddings colored by assigned bit-width.

## 6.4 Limitations and Future Directions

### 6.4.1 Current Limitations

RAMP was evaluated exclusively on decoder-only Transformer architectures (Llama and Mistral families). Its applicability to encoder-decoder models (e.g., T5, mT5) and mixture-of-experts architectures remains untested. The method currently supports only discrete bit-widths {3, 4, 5, 6} compatible with existing kernels; fractional or mixed-precision formats (e.g., 2.5-bit, 3.5-bit) are unsupported. Quantization occurs at layer granularity; finer head-level or channel-level allocation could yield further gains but requires corresponding kernel support. RAMP operates in the post-training setting only; integration with quantization-aware training could recover additional accuracy at aggressive compression levels. Although the policy transfers zero-shot, calibration (embedding extraction) must be repeated per model. Finally, bit allocations are static; input-dependent dynamic quantization is left for future work.

### 6.4.2 Future Directions

Potential extensions include:

- Cross-architecture transfer to encoder-decoder and non-Transformer models, requiring architecture-agnostic state representations.
- Head- or channel-level mixed precision, contingent on kernel support for intra-layer variable bit-widths.
- Integration with quantization-aware training to reach sub-3-bit regimes.
- Input-adaptive dynamic policies that adjust bits at inference time.
- Multi-objective optimization jointly targeting perplexity, latency, power, and size.
- Hardware co-design of kernels optimized for RAMP’s typical bit distributions.
- Hybrid sparsity-plus-quantization pipelines.

Table 15. Results on Mistral-7B

Method	Size (GB)	PPL	Size vs RAMP	PPL vs RAMP
FP16	14.5	5.45	+299%	—
GPTQ-4	3.85	5.71	+6.1%	+2.7%
AWQ-4	3.85	5.59	+6.1%	+0.5%
Q4_K_M	3.90	5.60	+7.4%	+0.7%
Direct SAC	3.62	5.58	-0.3%	+0.4%
<b>RAMP (zero-shot)</b>	<b>3.63</b>	<b>5.56</b>	—	—

Table 16. Zero-shot transfer summary

Target	Direct PPL	Direct Bits	Zero-shot PPL	Zero-shot Bits	Winner
Llama-2-13B	4.96	3.66	4.95	3.66	Zero-shot
Mistral-7B	5.58	3.67	5.56	3.67	Zero-shot

- Continual adaptation of policies for incrementally trained or fine-tuned models.

## 7 CONCLUSION

RAMP learns transferable mixed-precision quantization policies via reinforcement learning, achieving Pareto-optimal accuracy-efficiency trade-offs while enabling deployment through standardized GGUF formats.

### 7.1 Key Contributions

The main contributions are:

1. Demonstration of the first transferable quantization policy for LLMs: a policy trained on Llama-2-7B generalizes zero-shot to Mistral-7B and Llama-2-13B, often yielding lower perplexity than policies trained directly on the target.
2. Scale Folding, a preconditioning technique that stabilizes activation distributions and enables reliable sub-4-bit quantization.
3. A quality-prioritized reward with asymmetric penalties and cliff constraints that drives rapid, stable convergence of the SAC agent.
4. Strictly superior Pareto frontiers: on Llama-2-7B, RAMP reaches 5.54 PPL at 3.68 GB versus AWQ’s 5.60 PPL at 3.90 GB (6% smaller and 1.1% higher quality); comparable gains hold across Llama-3-8B and Mistral-7B.
5. HALO, a hardware-aware export pipeline that produces GGUF models runnable on CPUs, GPUs, Apple Silicon, and select edge devices without custom kernels.

### 7.2 Outlook

RAMP establishes that quantization sensitivity is largely a structural property of Transformer architectures rather than model-instance specific. This insight suggests that reinforcement-learned policies may generalize to other compression techniques (pruning, sparsity, distillation) and opens a path toward general quantization agents that map any model and efficiency target to an optimal quantized artifact.

## 8 BROADER CONTEXT AND IMPACT

RAMP enables practical mixed-precision deployment on consumer and edge hardware via standardized `llama.cpp` backends. A single GGUF artifact runs unmodified across NVIDIA/AMD GPUs, x86 CPUs, Apple Silicon, and some mobile platforms, reducing the barrier between research prototypes and real-world inference.

Model compression also lowers energy consumption. Illustrative estimates for 8 h/day inference of a 7B-class model show that RAMP-quantized execution on consumer hardware can reduce annual carbon emissions by 66–75% relative to cloud A100 baselines (see Table 23 for assumptions and order-of-magnitude calculations).

Assumptions: US grid intensity 0.4 kg CO<sub>2</sub>/kWh, \$0.10/kWh cloud pricing, public TDP and benchmark power draws. These are order-of-magnitude estimates, not direct measurements.

### 8.1 Future of Efficient LLM Deployment

Further gains are expected from hybrid sparsity-plus-quantization, input-adaptive policies, and hardware co-design of mixed-precision kernels. The long-term goal is a general quantization agent capable of mapping arbitrary models and efficiency targets to optimal compressed artifacts across diverse hardware.

Table 17. Commonsense reasoning performance (Llama-2-7B)

Method	PIQA	HellaSwag	WinoGrande	ARC	Avg
FP16	79.4%	58.2%	64.0%	53.9%	63.9%
AWQ-4	78.8%	57.1%	62.3%	52.4%	62.7%
Q4_K_M	78.6%	56.9%	62.1%	52.1%	62.4%
<b>RAMP</b>	<b>79.2%</b>	<b>57.9%</b>	<b>63.7%</b>	<b>53.6%</b>	<b>63.6%</b>
Retention vs. FP16	99.7%	99.5%	99.5%	99.4%	<b>99.5%</b>

Table 18. Embedding stability: Pearson correlations across models

Layer Role	Llama-2-7B	Llama-2-13B	Mistral-7B	Correlation
Embedding layer	(0.87, 0.34, 0.12, ...)	(0.91, 0.36, 0.13, ...)	(0.85, 0.32, 0.11, ...)	$r = 0.94$
Attention o_proj	(3.12, 0.18, 0.08, ...)	(3.15, 0.19, 0.09, ...)	(3.08, 0.17, 0.07, ...)	$r = 0.96$
MLP down_proj	(2.87, 0.22, 0.11, ...)	(2.91, 0.23, 0.12, ...)	(2.84, 0.21, 0.10, ...)	$r = 0.95$
Output layer	(1.24, 0.41, 0.19, ...)	(1.28, 0.42, 0.20, ...)	(1.21, 0.40, 0.18, ...)	$r = 0.93$

Table 19. Scale folding ablation

Configuration	Episodes to Conv.	Final PPL	Stable?
No folding	> 250	5.58	Partial
With folding	150	5.54	✓

Table 20. Reward ablation

Reward	Episodes to Conv.	Final PPL	Variance
Naive (Acc - $\lambda$ Bits)	$\infty$	> 5.75	0.35
Linear	200	5.61	0.18
Quality-first (asymmetric + cliff)	150	5.54	0.05

Table 21. SAC vs. PPO

Algorithm	GPU Hours	Final PPL	Variance
PPO	48	5.62	0.15
SAC	6	5.54	0.03

Table 22. HALO vs. custom kernels

Approach	Throughput	Portability / Effort
Custom mixed-precision kernels	Highest (hardware-specific)	Low (high engineering)
HALO / GGUF	Competitive	High (zero custom dev, broad hardware)

Table 23. Illustrative annual energy and carbon footprint (7B model, 8 h/day)

Deployment	Power (W)	Annual kWh	CO <sub>2</sub> (kg)	Cost (\$)
Cloud A100	350	2,920	1,168	292
RTX 3090 FP16	250	2,088	835	209
<b>RTX 3090 RAMP</b>	<b>85</b>	<b>711</b>	<b>284</b>	<b>71</b>
Xeon CPU RAMP	65	546	218	55
M1 laptop RAMP	12	101	40	10

## REFERENCES

- Meta AI. The llama 3 herd of models. *arXiv preprint arXiv:2407.21783*, 2024.
- Yonatan Bisk, Rowan Zellers, Jia Gao, and Yejin Choi. Piqa: Reasoning about physical commonsense in natural language. In *Proceedings of the AAAI Conference on Artificial Intelligence*, volume 34, pages 7432–7439, 2020.
- Hao Mark Chen, Fuwen Tan, Alexandros Kouris, Royson Lee, Hongxiang Fan, and Stylianos I. Venieris. Progressive mixed-precision decoding for efficient llm inference. In *Proceedings of the Thirteenth International Conference on Learning Representations*, 2025. URL <https://arxiv.org/abs/2410.13461>.
- Peter Clark, Isaac Cowhey, Oren Etzioni, Tushar Khot, Ashish Sabharwal, Carissa Schoenick, and Oyvind Tafjord. Think you have solved question answering? try arc, the ai2 reasoning challenge. In *arXiv preprint arXiv:1803.05457*, 2018.
- Zhen Dong, Zhewei Yao, Amir Gholami, Michael W Mahoney, and Kurt Keutzer. Hawq: Hessian aware quantization of neural networks with mixed-precision. In *IEEE/CVF Conference on Computer Vision and Pattern Recognition*, pages 293–302, 2020.
- Aamir T Elthakeb, Preetum Pilligundla, Amir Yazdanbakhsh, Mark A Kinsy, Sherief Reda, and Azalia Mirhoseini. Releq: An automatic reinforcement learning approach for deep quantization of neural networks. In *Proceedings of Machine Learning and Systems*, volume 1, pages 218–232, 2019.
- Elias Frantar, Saleh Ashkboos, Torsten Hoefler, and Dan Alistarh. Gptq: Accurate post-training quantization for generative pre-trained transformers. *arXiv preprint arXiv:2210.17323*, 2023.
- Leo Gao, Jonathan Tow, Stella Biderman, Sid Black, Anthony DiPofi, Charles Foster, Liane Golding, Jeffrey Hsu, Kyle McDonell, Niklas Muennighoff, et al. A framework for few-shot language model evaluation. In *arXiv preprint arXiv:2104.07567*, 2021.
- Tuomas Haarnoja, Aurick Zhou, Pieter Abbeel, and Sergey Levine. Soft actor-critic: Off-policy maximum entropy deep reinforcement learning with a stochastic actor. In *International Conference on Machine Learning*, pages 1861–1870, 2018.
- Yihui He, Xiangyu Zhang, and Jian Sun. Learning efficient convolutional networks through network slimming. In *IEEE International Conference on Computer Vision*, pages 2755–2763, 2017.
- Benoit Jacob, Skirmantas Kligys, Bo Chen, Mingxing Zhu, Matthew Tang, Andrew Howard, Hartwig Adam, and Dmitry Kalenichenko. Quantization and training of neural networks for efficient integer-arithmetic-only inference. In *IEEE/CVF Conference on Computer Vision and Pattern Recognition*, pages 2704–2713, 2018.
- Albert Q Jiang, Alexandre Sablayrolles, Arthur Mensch, Chris Bamford, Devendra Singh Chaplot, Diego de las Casas, Florian Bressand, Gregoire Lengyel, Guillaume Lample, Lucile Saulnier, et al. Mistral 7b. *arXiv preprint arXiv:2310.06825*, 2023.
- Jung Hyun Lee, Jeonghoon Kim, June Yong Yang, Se Jung Kwon, and Eunho Yang. LRQ: Optimizing post-training quantization for large language models by learning low-rank weight-scaling matrices. In *Proceedings of the 2025 Conference of the North American Chapter of the Association for Computational Linguistics*, 2025. URL <https://arxiv.org/abs/2407.11534>.
- Sehyun Lee, Jinsol Lee, Hyeongjun Kim, Gunho Kim, Eunhyeok Park, Jungwook Lee, Jung-Hoon Kim, Jaejin Kim, and Sunghyun Kim. Squeezellm: Dense-and-sparse quantization. In *International Conference on Machine Learning*, 2024.
- Ji Lin, Jiaming Tang, Haotian Tang, Shang Yang, Wei-Ming Chen, Wei-Chen Wang, Guangxing Xiao, Xing Dang, Chuang Gan, and Song Han. Awq: Activation-aware weight quantization for llm compression and acceleration. *arXiv preprint arXiv:2306.00978*, 2023.
- Qian Lou, Fenggang Guo, Minsoo Kim, Ling Liu, and Lei Jiang. Autoq: Automated kernel-wise neural network quantization. In *International Conference on Learning Representations (ICLR)*, 2020.
- Stephen Merity, Caiming Xiong, James Bradbury, and Richard Socher. Pointer sentinel mixture models. *arXiv preprint arXiv:1609.07843*, 2016.
- OpenAI. Gpt-4 technical report. *arXiv preprint arXiv:2303.08774*, 2023.
- Keisuke Sakaguchi, Rowan Le Bras, Chandra Bhagavatula, and Yejin Choi. Winogrande: An adversarial winograd schema challenge at scale. In *Proceedings of the AAAI Conference on Artificial Intelligence*, volume 34, pages 8732–8740, 2020.
- Wenqi Shao, Mengzhao Chen, Zhaoyang Zhang, Peng Xu, Lingfei Zhao, Zhiqiang Li, Kaipeng Zhang, Peng Gao, Yu Qiao, and Ping Luo. Omniquant: Omnidirectionally calibrated quantization for large language models. *arXiv preprint arXiv:2308.09066*, 2024.

Wei Tao, Haocheng Lu, Xiaoyang Qu, Bin Zhang, Kai Lu, Jiguang Wan, and Jianzong Wang. MoQAE: Mixed-precision quantization for long-context llm inference via mixture of quantization-aware experts. In *Proceedings of the 63rd Annual Meeting of the Association for Computational Linguistics*, 2025. URL <https://arxiv.org/abs/2506.07533>.

Hugo Touvron, Louis Martin, Kevin Stone, Peter Albert, Amaury Almahairi, Yasmine Babaei, Nikolay Bashlykov, Soumya Batra, Prajjwal Bhargava, Shruti Bhosale, et al. Llama 2: Open foundation and fine-tuned chat models. *arXiv preprint arXiv:2307.09288*, 2023.

Jerry Tseng, Harshit Sreenivasan, Yunyi Chen, Tushar Agarwal, and Kurt Keutzer. Quip#: Even better llm quantization with hadamard incoherence optimization. *arXiv preprint arXiv:2402.10147*, 2024.

Guangxing Xiao, Ji Lin, Mickael Seznec, Hao Wu, Julien Demouth, and Song Han. Smoothquant: Accurate and efficient post-training quantization for large language models. *arXiv preprint arXiv:2211.10438*, 2023.

Xiangyang Xu, Wenshuo Liu, Ming Qin, Chao Ding, Chen Zhang, and Dacheng Li. Rdo-q: Rate-distortion optimization for quantization. *arXiv preprint*, 2022.

Rowan Zellers, Ari Holtzman, Hannah Rashkin, Yonatan Bisk, Ali Farhadi, Franziska Roesner, and Yejin Choi. Hellaswag: Can a machine really finish your sentence? In *Proceedings of the 57th Annual Meeting of the Association for Computational Linguistics*, 2019.

Jinhao Zhang, Yunquan Zhang, Daning Cheng, Jun Sun, and Zicheng Yan. Calm: A cka-guided adaptive layer-wise modularization framework for llm quantization. In *arXiv preprint arXiv:2512.16282*, 2025.

Zhen Zheng, Xiaonan Song, Chuanjie Liu, et al. Mixllm: Llm quantization with global mixed-precision between output-features and highly-efficient system design. In *Proceedings of the Thirteenth International Conference on Learning Representations*, 2025. URL <https://arxiv.org/abs/2412.14590>. Referred to as MixPE/MixLLM in literature.

Barret Zoph, Vijay Vasudevan, Jonathon Shimonovskiy, and Quoc V Le. Neural architecture search with reinforcement learning. In *International Conference on Learning Representations*, 2017.

## A 11-DIMENSIONAL EMBEDDING SPECIFICATION

The SAC policy conditions its decisions on a compact, fixed-dimensional state representation for each quantizable layer. This 11-dimensional embedding abstracts layer sensitivity, structural role, and sequential context while remaining approximately invariant to model scale through normalization and logarithmic scaling. The design enables zero-shot policy transfer across models of different sizes and slight architectural variations.

The 11 features are computed as follows:

Table 24. Specification of the 11-dimensional layer embedding used by the RAMP policy.

Dim	Feature	Computation / Definition
1	Normalized depth	$\frac{i}{n_{\text{layers}} - 1}$
2	Log input dimension	$\log_2(\text{in\_features}/16)$
3	Log output dimension	$\log_2(\text{out\_features}/16)$
4	Weight standard deviation	$\min(\text{std}(W) \times 10, 1.0)$
5	Weight mean magnitude	$\min(\mathbb{E}[ W ] \times 10, 1.0)$
6	Layer-type scalar	0.0 (Q/K/V proj.), 0.25 (output proj.), 0.5 (gate proj.), 0.6 (up proj.), 0.75 (down proj.), 1.0 (otherwise)
7	Position category	0.0 (early: bottom 10%), 0.5 (middle: 10–90%), 1.0 (late: top 10%)
8	Mean activation scale	$\min(\mathbb{E}[\text{act\_scales}] \times 100, 1.0)$
9	Max activation scale	$\min(\max(\text{act\_scales}) \times 1000, 1.0)$
10	Previous-layer bit-width	(previous $b$ normalized by 8; 0.0 for first layer)
11	Running average bit-width	(running average $b$ normalized by 8)

Activation scales are extracted by registering forward hooks on linear layers, forwarding 128 sequences from the WikiText-2 training split, and aggregating per-channel maximum magnitudes. Logarithmic scaling for dimensions, clipping to [0,1], and per-model normalization collectively promote size invariance, which is critical for cross-model generalization.

## B SAC HYPERPARAMETER CONFIGURATION

All experiments use a single, fixed SAC configuration without extensive hyperparameter tuning. The chosen values provide a good balance of sample efficiency, training stability, and policy expressivity for the sequential bit-allocation task.

SAC optimization hyperparameters are listed in Table 25, replay buffer details in Table 26, and network architectures in Table 27.

The optimization settings are summarized below:

Table 25. SAC optimization hyperparameters

Parameter	Value	Notes
Learning rate	$3 \times 10^{-4}$	Shared across actor, critics, and temperature optimizer
Optimizer	Adam	Applied to all components
Discount factor $\gamma$	0.99	Standard for episodic tasks
Target update rate $\tau$	0.005	Ensures slow tracking of target networks
Gradient clipping norm	1.0	Prevents exploding gradients
Target entropy	-1	For single-dimensional continuous action
Initial entropy coefficient $\alpha$	$\exp(\log 0.2)$	Log-parameterized starting value

Replay buffer and training schedule:

*Table 26. Replay buffer and training schedule*

<b>Parameter</b>	<b>Value</b>	<b>Notes</b>
Batch size	128	Used for all gradient updates
Replay buffer capacity	30,000 transitions	Sufficient for $\sim 120$ episodes $\times$ 250 steps
Warm-up episodes	20	Purely random actions before policy gradients
Maximum episodes	200–300	Typical convergence budget in experiments

Actor and critic network architectures:

*Table 27. Actor and critic network architectures*

<b>Component</b>	<b>Architecture</b>	<b>Notes</b>
Actor	FC-512-LN-ReLU $\rightarrow$ FC-512-LN-ReLU $\rightarrow$ FC-256-ReLU $\rightarrow$ FC-2	Outputs mean and log-std of action
Critic (twin)	FC-512-LN-ReLU $\rightarrow$ FC-512-LN-ReLU $\rightarrow$ FC-256-ReLU $\rightarrow$ FC-1	Input is state concatenated with continuous action
Hidden activation	ReLU	Fast and effective for policy/value approximation
Normalization	LayerNorm	Applied after the first two hidden layers

These choices were empirically stable across all evaluated models and did not require per-model retuning.